

Irradiated Planets

Travis S. Barman, Peter H. Hauschildt

*Dept. of Physics and Astronomy & Center for Simulational Physics, University of Georgia,
Athens, GA 30602-2451*

Email: travis@hal.physast.uga.edu, yeti@hal.physast.uga.edu

France Allard

C.R.A.L (UML 5574) Ecole Normale Supérieure, 69364 Lyon Cedex 7, France

E-Mail: fallard@ens-lyon.fr

ABSTRACT

We have modeled irradiated planets located near a dM5 and a G2 primary star. The impinging radiation field was explicitly included in the solution of the radiative transfer equation and in the computation of the atmospheric structure. We find that large errors in both the thermal and reflected flux will result from models which do not include the impinging radiation in a self-consistent manner. A cool ($T_{\text{eff}} = 500\text{K}$) and a hot ($T_{\text{eff}} = 1000\text{K}$) planet were modeled at various orbital separations from both the dM5 and the G2 primary. In all scenarios, we compared the effects of the irradiation in two extreme cases: one where dust clouds form and remain suspended in the atmosphere, and another where dust clouds form but completely settle out of the atmosphere. The atmospheric structure and emergent spectrum strongly depend on the presence or absence of dust clouds. We find that, in the absence of dust opacity, the impinging radiation significantly alters the innermost layers of an EGP atmosphere and that they are actually brighter in the optical than dusty planets. Our models also indicate that the planet-to-star brightness ratio in the optical will be less than 1×10^{-5} for objects like τ bootis which is consistent with recently reported upper limit values.

Subject headings: stars: planetary systems, stars: atmospheres, radiative transfer

1. Introduction

Many indirect detections of substellar objects in close orbit around stars of spectral type later than F have been made since 1996. However, currently there are few observations that can be useful for constraining the large parameter space (e.g. chemical composition, albedo, age, and inclination) for any of these so called extra-solar giant planets (EGPs). The transits observed for HD209458a by Henry et al. (2000) and Charbonneau et al. (2000) have helped constrain the gross physical parameters of HD209458a (radius, mass, mean density, etc.) but not any of the atmospheric properties. There is great hope that the handful of ambitious space and ground based projects planned for the next decade will be capable of making direct photometric observations of EGPs and possibly measurements of EGP spectral features. Until then, we must rely on atmospheric modeling to provide insight into the basic properties of these objects to guide the observers while we wait patiently for their observations.

An early work by Saumon et al. (1996) investigated the properties of EGPs for various masses and ages near primaries of different spectral type but approximated the reflected and thermal flux as gray bodies. More recently there have been several radiative equilibrium models produced for the purpose of predicting certain observables for 51 Pegasi B (Seager & Sasselov 1998) and τ Boo (Goukenleuque et al. 2000). Also, a broad range (100 – 1700K) of EGP models were studied and loosely classified by Sudarsky et al. (2000) using ad hoc temperature – pressure profiles. In this paper, we present equilibrium models for several scenarios well within the known parameter space for EGPs. We have investigated the variations of the thermal structures and emergent flux as functions of both the spectral type of the primary and the orbital separation. We also address the importance of spherical versus plane parallel radiative transfer. Our emphasis in this paper is not on any one particular EGP, but instead on the basic understanding of these objects and the effects of their close proximity to a stellar companion.

2. Model Construction

We have used our multi-purpose atmosphere code PHOENIX (version 10.9) to generate the models discussed below. Most details of the radiative transfer method may be found in Hauschildt & Baron (1999), but, for clarity, we repeat some of the basic features and discuss a few changes needed for irradiated models. PHOENIX solves either the full spherically symmetric or plane parallel radiative transfer equation (PPRTE) using an operator splitting (OS) technique. For the majority of the calculations presented here, we have chosen plane parallel geometry and assumed hydrostatic equilibrium. However, we will discuss the impor-

tance of spherical geometry in section 4. All models are subject to an energy conservation constraint such that the total Flux (convective and radiative) is constant at each layer. Each model atmosphere spans a range of optical depth (τ_{std} defined at $1.2\mu\text{m}$) from 0 at the top of the atmosphere down to 100 at the deepest layer. Convection is treated according to the Mixing Length Theory from the onset of the Schwarzschild criterion with mixing length parameter, $\alpha = 1$.

The usual boundary conditions for an isolated star are that the inward directed flux at the surface should be zero ($I_{\nu}^{\downarrow}(\tau_{std} = 0, \mu) = 0$, where $-1 \leq \mu = \cos(\theta) \leq 0$) and that the diffusion approximation holds at the bottom of the atmosphere. For a close binary, the situation is clearly different. At the surface of the secondary, the boundary condition on I_{ν}^{\downarrow} is determined by the incident flux (F_{ν}^{inc}) given by:

$$2\pi \int_{-1}^0 I_{\nu}^{\downarrow}(\mu) \mu d\mu = F_{\nu}^{\text{inc}}(\tau_{std} = 0) \quad (1)$$

where

$$F_{\nu}^{\text{inc}}(\tau_{std} = 0) = \left(\frac{R^{\star}}{a}\right)^2 F_{\nu}^{\star} \quad (2)$$

In the equations above, $I_{\nu}^{\downarrow}(\mu)$ refers to the inward directed intensities along direction μ , R^{\star} is the radius of the primary, a is the surface to surface primary-secondary separation, and F_{ν}^{\star} is the monochromatic flux from the primary. For F_{ν}^{\star} , we use a synthetic spectrum taken from a previous PHOENIX calculation (Hauschildt et al. 1999; Allard et al. 2000). For the models presented below, we have made the simplifying assumption that the impinging radiation field is isotropic, meaning that $I_{\nu}^{\downarrow}(\mu)$ at the surface is the same for all μ (i.e., $I_{\nu}^{\downarrow}(\mu) = I_{\nu}^{\downarrow}$). We have also assumed that the flux is *not* globally redistributed over the planet’s surface. A more detailed discussion of these last two issues may be found in section 4.

As was done in the work on irradiated M Dwarfs by Brett & Smith (1993), all of the incident radiation from the primary is re-radiated outward by the secondary in the form of reflected flux (F^{ref}) and as a contribution to the thermal flux (F^{therm}). This constraint is required by energy conservation and implies that the integrated flux at the surface is equal to $\sigma T_{\text{int}}^4 + F^{\text{inc}}$. Throughout this paper, T_{int} refers to the effective temperature of the planet in the *absence* of irradiation and $4\pi R_p^2 \sigma T_{\text{int}}^4$ equals the planet’s intrinsic luminosity where R_p is the planet’s radius. The intrinsic luminosity is an age dependent quantity which represents the energy released by the planet as it cools and contracts. T_{int} also relates irradiated planets to isolated planets in which case T_{int} is identical to the more commonly used T_{eff} .

The “effective temperature” (T_{eff}), which is customarily defined as the temperature a black body would have to have in order to radiate the total flux, has important physical and

observational significance for isolated stellar and substellar objects. However, for irradiated planets (and stars) T_{eff} loses some of its connection to the fundamental properties of the planet because it is difficult to separate, by observation, those photons which are thermally radiated by the planet from those which originated from the primary and are merely reflected by the planet. We shall only use T_{eff} , with its customary definition, to describe non-irradiated objects. When describing irradiated objects, we will define another quantity which describes the equilibrium temperature of the planet’s day side;

$$\sigma T_{\text{eq}}^4 = \sigma T_{\text{int}}^4 + (1 - A_B)F^{\text{inc}}, \quad (3)$$

where A_B is the Bond albedo. Since the reflected flux is not directly related to the equilibrium thermal structure of the atmosphere, it has been omitted from equation 3 and, therefore, distinguishes T_{eq} from T_{eff} . It is also important to realize that T_{eq} , as defined above, represents the equilibrium state at a given age and allows for the possibility that the intrinsic luminosity has not reached zero. T_{int} will only be important for young (or more massive) planets when the primary is a solar type star. However, for planets orbiting M dwarfs, T_{int} can be a significant contribution to T_{eq} . While T_{eq} , which likely varies across the planet’s day side, tells us little about the interior or the non-irradiated face of the planet it does provide a useful measure of the effects on the thermal structure of the planet’s day side. It is also important to realize that T_{int} is not necessarily the equilibrium temperature of the planet’s night side since energy may be carried over from the day side.

To produce an irradiated atmospheric model, we chose the structure of a converged non-irradiated model taken from Allard et al. (2001) as the initial structure of an irradiated atmosphere located $\sim 5\text{AU}$ from the primary. At this distance, the impinging radiation produces only small changes in the structure of the upper layers and convergence is achieved after only a few iterations. This new model is then used as the initial structure for an irradiated atmosphere located at $\sim 2.5\text{AU}$ from the primary. This process of moving the planet closer to the primary is repeated until the desired orbital separation is reached. Each intermediate calculation is iterated until the changes to the temperature structure are less than 1 K at every depth point and energy conservation is satisfied to within a few percent. Models obtained in this way will have structures, at the deepest layers, similar to the initial non-irradiated model chosen from Allard et al. (2001), and thus depend on $\log(g)$, and the assumed value of T_{int} .

The opacity setups used for the EGPs are identical to the “AMES-Cond” and “AMES-Dusty” models of Allard et al. (2001) which refer to two limiting cases. AMES-Cond refers to the situation when dust forms in the atmosphere at locations determined by the chemical equilibrium equations, but has been entirely removed from the atmosphere by efficient gravitational settling. Dust formation, therefore, acts only to remove refractory elements

and reduce the number of certain molecules but does *not* contribute to the overall opacity. The opposite case, AMES-Dusty, ignores settling altogether. Dust forms based on the same criteria as in the AMES-Cond models yet remains present to contribute to the opacity. The Cond model may be thought of as “clear skies”, and the Dusty model as “cloudy skies”.

The opacities include H₂O and TiO lines by Partridge & Schwenke (1997), CH₄ lines from the HITRAN and GEISA databases (Rothman et al. 1992; Husson et al. 1992), and H₂, N₂, Ar, CH₄, and CO₂ collision induced absorption (CIA) opacities according to (Borysow et al. 1997a,b; Borysow & Frommhold 1986a, 1987a, 1986b; Borysow & Tang 1993; Samuelson et al. 1997; Borysow & Frommhold 1986c, 1987b; Gruszka & Borysow 1997, and references therein). To include dust grains, we have assumed an interstellar size distribution with diameters ranging from 0.00625 to 0.24 μ m and the chemical equilibrium equations incorporate over 1000 liquids and crystals (Allard et al. 2001). We follow the prescriptions of Grossman (1972) and use Gibbs free energies of formation from the JANAF database (Chase et al. 1985) to compute the number densities for each grain species. The condensation equilibrium is directly incorporated into the chemical equilibrium equations to account, self-consistently, for the depletion of refractory elements as a function of gas temperature and pressure. With this approach, any changes to the structure brought on by irradiation will be automatically accounted for in the chemical equilibrium equations.

3. Results

We have divided our study into two separate cases: one for which the primary star is a dM5 ($T_{\text{eff}} = 3000\text{K}$, see Leggett et al. (2000); Allard et al. (2000)) and another where the primary is a G2 solar type star ($T_{\text{eff}} = 5600\text{K}$, see Hauschildt et al. (1999)). For the former case, one finds few observed objects in the literature (eg Gl876B). However, surveys for additional objects have begun (Delfosse et al. 1999) . In the last decade, most of the observations have been spent searching for objects that fall into the second group, and, to date, there are roughly 50 planets known to be in orbit around solar type stars. For both of these cases, we consider different effective temperatures and several orbital separations. Below, we present the structures and spectra for each case and discuss the effects caused by the impinging radiation.

3.1. EGPs Around M Dwarfs

Gl876B was the first planetary companion found orbiting an M dwarf. This was an important discovery given that M dwarfs constitute nearly 70% of all stars in the galaxy (Henry 1998). Gl876B is also one of the nearest EGPs (only 5 pc away) making it a promising candidate for direct imaging by future adaptive optics and interferometry missions (Marcy et al. 1998). Our first group of irradiated models is intended to represent objects, like Gl876B, which have cool stellar primaries. We begin with a planet having $T_{\text{int}} = 500\text{K}$, $R_p = 1R_{\text{jup}}$ and $\log(g) = 3.5$ located very close to a dM5. Both planet and primary have solar compositions.

In Figure 1, we show the temperature structure of the non-irradiated planet compared to irradiated thermal structures at 0.1 and 0.05AU for both the AMES-Cond and AMES-Dusty cases. The outermost regions are significantly altered by the radiation from the dM5 resulting in a generally flatter temperature profile. Without dust opacity (the AMES-Cond model), the impinging radiation is capable of heating the lower layers of the planet thereby reducing the temperature gradient. Above the photosphere ($\tau_{\text{std}} < 10^{-4}$), the largest temperature increase occurs and a very slight temperature inversion forms at 0.05AU. Dust opacity generally produces a hotter atmosphere at all depths with a smoother spectral energy distribution. For more details on the effects of dust in non-irradiated atmospheres, see Allard et al. (2001). It is important to stress that the solution of the chemical equilibrium equations is based on the final temperature structure and thus incorporates the irradiation effects.

In the AMES-Dusty models, Fe, Mg_2SiO_4 , MgSiO_3 and $\text{CaMgSi}_2\text{O}_6$ and MgAl_2O_4 are the dominant dust species which form a cloudy region extending from roughly $\tau_{\text{std}} = 1.0$ to the top of the atmosphere. Below this region ($\tau_{\text{std}} > 1.0$) is a complicated mixture of various other condensates. In Figure 2, the concentrations of the dominant dust species are shown for the irradiated and non-irradiated planets. There is little change in the abundance of the condensates brought on by the impinging radiation from the dM5.

The spectra for the irradiated and non-irradiated planets are shown in Figure 3. The isolated AMES-Dusty planet produces a very smooth spectrum in the optical as is expected for an atmosphere dominated by grain opacity. In the IR, several distinct molecular bands are present: CH_4 at $1.6\mu\text{m}$, $2.1 - 2.5\mu\text{m}$, and $3.0 - 4.0\mu\text{m}$, and H_2O between 2.5 and $3.0\mu\text{m}$. The reflective properties of the dust between the near-UV and the near-IR is clearly shown in the spectrum of the irradiated AMES-Dusty planet. Even at 0.1AU, the planet reflects a considerable amount of radiation in the optical bands compared to the non-irradiated planet. However, the ratio (ϵ) of the planet flux to that of the incident flux is quite small. Averaged over 4500 to 5200Å, ϵ is about 10^{-7} for the AMES-Dusty at 0.05AU. In the IR, the flux also increases and the molecular bands become progressively shallower as the planet approaches

the primary. The increase in flux at infrared wavelengths is *not* due to reflection, but is entirely a thermal effect.

The effects of irradiation on the spectrum of the 500K AMES-Cond planet are also shown in Figure 3. Distinct molecular bands, primarily due to water and methane, are clearly visible for $\lambda > 1\mu\text{m}$. These bands are sensitive to the temperature at various depths. The methane absorption (at $\sim 1.8\mu\text{m}$, $2.2 - 3.0\mu\text{m}$ and $3.1 - 4.0\mu\text{m}$) probes the deeper layers and indicates that, up to 0.1AU, little change in the temperature has taken place in the photosphere. Once 0.05AU separation has been reached, the irradiation has produced a much larger temperature rise resulting in nearly an order of magnitude increase in the emerging flux at $3.5\mu\text{m}$. Similarly, the water bands (at $0.9\mu\text{m}$, $1.1\mu\text{m}$ and $1.4\mu\text{m}$) probe the upper layers and are sensitive to the irradiation even at 0.1AU. The AMES-Cond model also produces a reflected component in the UV and optical regions, though less dramatic than in the Dusty model when compared to the non-irradiated planet’s intrinsic flux. In this case, $\epsilon = 3.6 \times 10^{-6}$ at 0.05AU, which is roughly 10 times that seen in the Dusty model.

It is quite possible that many of the young EGPs have T_{int} closer to that of an L or T dwarf. To investigate this possibility, we have modeled an EGP with $T_{\text{int}} = 1000\text{K}$ (all other parameters are the same as for the above 500K planet) irradiated by the same dM5 used above. The results are qualitatively similar but weaker, for both the Cond and Dusty situations, than those of the previous cooler planets. So, in order to explore the regime where irradiation effects become important, we must study these planets at even smaller orbital separations. Figures 4 and 5 demonstrate the effects of irradiation on the structure and spectrum, respectively, for the 1000K AMES-Dusty and AMES-Cond models. As with the cooler dusty planet, the inner regions are not affected by the irradiation even at 0.005 AU ($\sim 1R_{\odot}$), a separation more common in cataclysmic variables. The AMES-Dusty spectrum (Fig. 5) is featureless in the IR for separations $< 0.01\text{AU}$, but many of the absorption lines present in the dM5 are now reflected in the optical spectrum of the planet. The AMES-Cond planet experiences a significant temperature increase at all photospheric layers (Fig. 4) and a suppression of the convective zone also seen in the cooler AMES-Cond planet. The spectra (Fig. 5) show several orders of magnitude increase in the flux for the methane and water bands at 0.01AU with many reflected atomic features in the optical when the Cond planet is at 0.005AU from the primary.

3.2. EGPs Around Solar Type Stars

Many EGPs have been discovered orbiting solar type stars (e.g., 51 Peg B), and have already received much attention in the literature in both observational and theoretical studies.

Recent works include models of 51 Peg B (Goukenleuque et al. 2000), HD209458a (Seager & Sasselov 2000) and a study of EGP photometric and polarization properties (Seager et al. 2000). We have taken a slightly more general approach; we do not focus on any one particular known object. We have chosen, instead, a planet with $T_{\text{int}} = 500\text{K}$ and a young planet with $T_{\text{int}} = 1000\text{K}$ orbiting an object similar to the Sun as average representatives of most currently known EGPs orbiting F, G, and K stars.

Figure 6 demonstrates the effects of impinging radiation from a G2 primary on the 500K AMES-Cond and AMES-Dusty atmospheric structure for several separations. As in the dusty cases presented above, the inner part of the AMES-Dusty atmosphere is unaffected by the irradiation. However, regions around $\tau_{\text{std}} \sim 10^{-4}$ show a dramatic rise in temperature as the planet is moved from 1.0 to 0.3AU. At 0.3AU, the Dusty model reaches $T_{\text{eq}} = 767\text{K}$ and the temperature in the upper atmosphere ($\tau_{\text{std}} < 10^{-4}$) has more than doubled. Also at 0.3AU, the AMES-Cond model reaches $T_{\text{eq}} = 735\text{K}$ and, for regions near $\tau_{\text{std}} = 1$, the temperature has risen by over 150K. Even the deepest layers feel the presence of the primary. The temperature at $\tau_{\text{std}} = 10$ increases by 100K, and the boundary between the radiative and convective zone, which was well above $\tau_{\text{std}} = 1$ at 1.0AU, has retreated to nearly $\tau_{\text{std}} = 50$. Large concentrations of dust species are still capable of forming in the upper atmosphere. In the AMES-Dusty model, at 0.15AU, there still remains a thick cloudy region with concentrations similar to those seen in the 500K planet near a dM5 (see Fig. 2). The only major difference being Fe which extends to the upper regions where $\log(P_{\text{gas}}) \sim 1.0$ dynes cm^{-2} .

The optical and IR regions of the spectrum for each orbital separation are shown in Figure 7 where the differences between the AMES-Dusty and AMES-Cond models can clearly be seen. The dusty models produce very smooth spectra except for the reflected features in the optical bands. The dust is entirely responsible for the reflection effects in this case. As the dusty planet is brought closer to the G2, the few absorption features (primarily CH_4) seen in the non-irradiated planet completely disappear. At 0.5AU, very little change has taken place for $\lambda > 7000\text{\AA}$ in the Cond model spectrum and the water and methane bands remain strong. However, for $\lambda \leq 7000\text{\AA}$, a large amount of reflected light is already present even at 0.5AU. As the planet is brought closer to the primary, the reflected light around 5000\AA steadily increases. Nearly all ($\sim 95\%$) of the light reflected by the Cond model is due to Rayleigh scattering by the two most abundant species, H_2 and He. At 0.3AU nearly 10^7 times more light emerges from the planet around 5000\AA , however it remains very faint compared to the incident radiation with $\epsilon = 2 \times 10^{-7}$ between 4500 and 5200\AA .

The younger $T_{\text{int}} = 1000\text{K}$ planet behaves in a similar manner as in the cases near a dM5 presented in section 3.1. The structure of the AMES-Cond planet, displayed in

Figure 8, shows a significant suppression of the convective zone (below $\tau_{std} = 10$ at 0.05AU) and the temperature has increased by a factor of 3 at $\tau_{std} = 10^{-4}$. The Dusty model also shows a large temperature inversion above $\log(P_{gas}) = 3.0$ dynes cm^{-2} . As can be seen in Figure 9, the Dusty model at 0.15AU exhibits a complex mixture of cloud species throughout the atmosphere. Fe, Mg_2SiO_4 , and MgSiO_3 are the most prominent species except for the deeper layers where $\text{CaMgSi}_2\text{O}_7$ begins to dominate. The spectra, shown in Figure 10, display similar results as in the previous cases. However, at 0.05AU, the molecular bands have nearly disappeared in the Cond model and the once broad Na I and K I doublets (5890 and 7680Å) are extremely weak. Figure 11 shows, in more detail, the steady reduction in equivalent width of both lines for the AMES-Cond models. The decrease in equivalent width is almost entirely due to the changes in thermal structure shown above. At 0.05AU, the Cond planet has reached $T_{eq} = 1752\text{K}$.

4. Discussion

4.1. Importance of Self-consistent Models

Many previous studies have used the structures of a non-irradiated planets with $T_{eff} = T_{eq}$ and simply computed a spectrum (or albedo) which included the incident flux and neglected the effects on the structure and chemical composition (Marley et al. 1999). This procedure will, however, result in gross errors in the emergent flux from the optical to infrared. In Figure 12, we compare the thermal spectrum of the self-consistent irradiated (AMES-Cond, $T_{int} = 1000\text{K}$) planet at 0.065AU from a G2 star to that of a non-irradiated AMES-Cond model with an equal amount of thermal flux (i.e., $T_{eff} = T_{eq}$). Based on the irradiated spectrum without the reflected component, we estimate that $T_{eq} = 1560\text{K}$. The non-irradiated model significantly underestimates the flux in the water and methane bands and overestimates the flux in the regions outside the molecular bands. Also, the non-irradiated model overestimates the amount of reflected light blueward of 6000Å by $\sim 35\%$. Atomic features are also affected as can be seen for the Na I D line (Fig. 12) where the equivalent width is overestimated in the non-irradiated model even when the reflected light is included in the spectrum calculation. The differences between the structures (see Fig. 13) are just as striking. As might be expected, the non-irradiated model is still cooler (by 350K) than the irradiated model in the upper atmosphere ($\tau_{std} \sim 10^{-4}$). At deeper layers the two structures actually intersect and, at $\tau_{std} \sim 10$, the non-irradiated model is *hotter* than the irradiated model by roughly 350K. An even more apparent difference is the location of the boundary between the radiative and convective regions. In the non-irradiated model, the convective zone reaches layers above $\tau_{std} = 1.0$ while in the irradiated case, the

convective zone has retreated to layers below $\tau_{std} = 10.0$. These differences, between a non-irradiated structure with $T_{\text{eff}} = T_{\text{eq}}$ and a structure based on a self-consistent inclusion of the impinging radiation, will have significant consequences for any interior and evolution calculations of irradiated planets.

4.2. Limiting Effects of Dust

The question of how much energy is redistributed by "weather patterns" is extremely important, and affects the upper boundary condition for irradiated models. To answer this question, 3D dynamical models of grain growth and diffusion would be needed. In this work, we explore the limiting effects of these patterns with Cond models, corresponding to clear skies, and Dusty models corresponding to cloudy skies. We find that irradiated Cond and Dusty models yield systematically different thermal spectra. The infrared spectra of Dusty and Cond planets around M dwarfs are affected by the impinging radiation only for extremely small orbits. However at separations around 0.05AU from a G2 star, the substellar point (the point on the planet closest to the star) will have a nearly featureless spectrum even in the Cond limit. The lack of spectral features is a consequence of the structure becoming nearly isothermal and is not a result of any significant decrease in abundances.

The emergent flux from both our irradiated and non-irradiated models indicates that Cond atmospheres are brighter at optical wavelengths than Dusty atmospheres. In general, Cond models are much brighter than the Dusty cases simply because the dust opacity blocks most of the thermal radiation (see Allard et al. (2001) for more details). When incident radiation is present, the dust grains reflect large amounts of light while continuing to block most of the *intrinsic* optical flux. Irradiated Cond atmospheres remain very transparent and allow large amounts of flux to emerge from the deep hotter layers. When this intrinsic thermal radiation is combined with the reflected flux, the irradiated Cond model appears brighter than the Dusty model.

The fraction of the stellar light reflected by our Cond model (at 0.05AU from a G2) around 4900Å is less than 5×10^{-6} . This is well below the results published by Cameron et al. (1999) and the upper limit published by Charbonneau et al. (1999). Also, the strong color dependence of Rayleigh scattering causes the reflected optical light (scattered by H₂ and He) in the Cond models to be considerably different from the optical spectrum of the primary. However, the reflected light in the Dusty atmospheres is due almost entirely to Mie scattering which is a fairly grey process. The result is a near reflected copy of the stellar optical spectrum. A comparison between the stellar light and the reflected optical spectrum for a $T_{\text{int}} = 1000\text{K}$ planet located at 0.15AU from a G2 primary can be seen in Figure

14. For wavelengths less than 4500\AA , the reflected light in the Dusty model matches closely the stellar light. At redder wavelengths, the two spectra differ not only in the slope of the continuum, but also in the depth of $H\alpha$ and the Na I doublet at 5890\AA . The Cond model has a very different optical spectrum with the redder wavelengths being dominated by an extremely broad Na I doublet (5890\AA). In general, the two spectra have little in common. Recent attempts have been made (Cameron et al. 1999; Charbonneau et al. 1999) to observe a Doppler shifted copy of the stellar light reflected by the planet orbiting τ_{std} Boo. Figure 14 suggests that planets in the Cond limit would be poor candidates for such techniques. Dusty planets, however, are clearly better choices and observations at shorter wavelengths may be more fruitful. In either case, observations similar to those of Cameron et al. (1999) and Charbonneau et al. (1999) could help determine the Cond or Dusty nature of EGPs.

4.3. Energy Redistribution

Clearly the fraction of the irradiated face seen by an observer depends on orbital phase and inclination. In addition, the planet’s atmospheric structure will likely vary across the planet’s surface. Guillot et al. (1996) claimed that one could assume that the radiation received by the planet’s day side is quickly redistributed over the entire planet surface. However, a recent calculation by Guillot (2000) indicates that this redistribution may take place over longer time-scales ($\sim 10^5$ seconds) than previously thought. This would imply that there exists, in those planets which are tidally locked, a large temperature difference between the day and night sides. Furthermore, if such a difference existed, the structure of the irradiated face would vary as a function of latitude and longitude and should approach the structure of the non-irradiated face for regions near the terminator¹. Therefore, it is unlikely that an irradiated planet can be characterized by a single 1-D plane parallel model atmosphere. Though it is reassuring that our results agree qualitatively with those of previous studies (Seager & Sasselov 1998; Seager et al. 2000; Goukenleuque et al. 2000), to accurately predict the spectrum and reflected light as a function of inclination and phase will require, at the very least, many 1-D models each accounting for the different amounts of energy deposited on the planet’s day side at various longitudes and latitudes. We are currently working on a sequence of non-isotropic irradiated models which include only the incident flux that a certain latitude² would receive. With such a sequence, we would be capable of modeling the

¹The terminator is the line dividing night and day on a planet.

²For this purpose, we assume that the symmetry axis is a line connecting the planet and primary. In this context, lines of constant latitude would refer to concentric rings about the substellar point.

reflected light for any phase and inclination.

Many of the recent studies (Marley et al. 1999; Seager & Sasselov 2000; Seager et al. 2000; Goukenleuque et al. 2000; Sudarsky et al. 2000) have made the assumption that the planet receives an amount of energy equal to $\pi R_p^2 F^{\text{inc}}$ which is quickly redistributed (Guillot et al. 1996) over the entire planet surface. As a result, these previous works have essentially included the minimum amount of external flux ($\frac{1}{4}F^{\text{inc}}$) that could be received by a planet at a given separation. If the more recent calculation by Guillot (2000) is correct and global redistribution is inefficient, then the models in these previous studies would be valid only for separations larger than what the authors had originally intended and only for a specific ring around the substellar point. In our calculations, we have assumed no redistribution and therefore have included a much larger amount of external flux (F^{inc}). Despite the assumption of an isotropic external radiation field, we feel that our models adequately represent the substellar point where this assumption is more reasonable.

4.4. Transmission Spectra

In the recent study by Seager & Sasselov (2000) an attempt was made to model the transmitted flux of HD209458a (recently shown to be an eclipsing system) through the upper regions of the planet’s atmosphere. Seager & Sasselov (2000) assumed that the structure at the poles (and along the terminator) was the same as that given by their fully irradiated model. However, the planet receives only a small amount of incident flux at the terminator and only in the upper atmosphere. In the absence of strong energy redistribution, the terminator would have a structure more closely resembling that of the non-irradiated face.

For a transmission study, one must calculate the stellar flux passing through a thin region at the top of the planet’s atmosphere ($\sim 0.01R_p$ thick) which includes latitudes above 82° . While, in general, EGPs are adequately described by plane parallel geometry, as one approaches the limb, the plane parallel assumption becomes increasingly less accurate. Using plane parallel geometry to calculate the transmitted spectrum assumes that the stellar flux passes through a region of constant thickness and height (a slab). In reality, the flux is passing through a section of a sphere encompassing the limb, in which case, rays entering at different latitudes will pass through different amounts of the planet’s atmosphere. A simpler and more accurate way of calculating the transmitted flux is to solve the spherically symmetric radiative transfer equation (SSRTE) and take, as the transmitted flux, the average intensities for direction cosines which pass through this band. The main advantage over the plane parallel solution is that the correct geometry is automatically built into the SSRTE. When solving the SSRTE, the atmosphere is modeled as a discrete number of concentric shells

surrounding the interior (or core). The transfer equation is then solved along characteristics which are divided into two categories: those which reach the core (core intersecting) and those which do not (tangential). Along a given characteristic, the direction cosine is now a function of depth whereas in the plane parallel case it is constant. Also, the diffusion approximation must hold at the inner boundary for the core intersecting characteristics but *not* for the tangential characteristics. The solution along the tangential characteristics which pass through the outer most shells is all that is needed to calculate the transmitted flux and will already account for the curvature of the limb.

Consider again the 1000K AMES-Cond planet located 0.05AU from a G2 primary and imagine that we observe the planet at (or near) inferior conjunction. Under such conditions one would observe a brighter planetary limb due to the transmitted stellar flux. In a spherically symmetric geometry, the effect emerges from the model in a very natural and physical manner. In Figure 15, we compare the transmitted flux for two different structures: our fully irradiated AMES-Cond structure ($T_{\text{eq}} = 1633\text{K}$) and the non-irradiated model ($T_{\text{eff}} = 1000\text{K}$). In both cases, the planet leaves its mark on the stellar flux as it passes through the planetary limb in the form of much stronger absorption features than seen in the unpolluted stellar spectrum. The transmitted spectrum based on the irradiated structure peaks at $3\mu\text{m}$, but the non-irradiated planet (see Fig. 10) is still 100 times brighter in this region and over 10^5 times fainter than the primary. In both cases, the planet’s limb is $\sim 10^3$ times brighter between 4500 and 5000Å than the planet’s night side. However, the disk of the G2 dominates the optical spectrum and is $\sim 10^6$ times brighter than the planet’s limb.

5. Conclusions

In this paper we have presented atmospheric models of planets in the presence of strong impinging radiation from primaries of different spectral type and at various orbital separations. We have also studied the effects of irradiation in two limiting cases: efficient settling (accounting for the depletion of elements by condensation) and complete cloud coverage.

Irradiation has only small effects on the atmospheres of planets with dM primaries except for extremely close orbits. For an object like Gl876B, which orbits a dM4 at 0.2AU, it is unlikely that any irradiation effects will be observed. However, for planets in the Cond limit orbiting G2 primaries, the effects are non-negligible. The upper layers of the atmospheres are significantly heated by the impinging radiation even at 0.5AU in both the Cond and Dusty limits. The inner layers of the Cond models also experience considerable heating and a suppression of the radiative-convective boundary. The innermost layers of the Dusty models are essentially unaffected by the irradiation even for close orbits. These results will

have strong implications for interior and evolution calculations. The heating of the inner layers in the Cond limit can bring the temperatures at the bottom of the atmosphere close to those in the Dusty limit. This would suggest that, in certain situations, the interior models would no longer depend on the Dust-Cond uncertainty published by Chabrier et al. (2000). However, it is still important that detailed interior and evolution models be calculated which use irradiated atmospheres to set upper boundary condition.

The existence of “weather patterns” on EGPs in the form of strong zonal winds and clear, cloudy or partly cloudy skies, will greatly influence the effects caused by irradiation. Our models indicate that an EGP with significant cloud coverage will reflect a copy of the stellar optical light while EGPs with clear skies will have very different reflected spectra. We have also found that young EGPs with clear skies are actually brighter in the optical than cloudy EGPs despite the more efficient reflective properties of dust. In general, our models indicate that observations would need to be sensitive to variations in the planet+star spectrum on the order of 10^{-5} to 10^{-6} in order to disentangle the reflected or transmitted flux.

It is apparent from observations of Jupiter and the other Jovian planets that clouds are *not* homogeneously distributed over the surface and that complex weather patterns persists. There is also evidence (from Galileo) that, unlike our simplified dusty models, clouds form in thin decks and any condensation occurring at the uppermost layers would soon “rain” out onto the lower atmosphere possibly instigating a cascade of diffusive settling (Encrenaz 1999). A self-consistent treatment of this behavior is currently being added to PHOENIX and results for both irradiated and non-irradiated atmospheres will be presented in future papers. Until these results are available, the models presented above are representatives of clear (AMES-Cond) and completely cloudy (AMES-Dusty) skies. It is possible to combine our Dusty and Cond models to investigate the intermediate “partly cloudy” cases.

Though it is unlikely that any of the models produced thus far are exact representations of a currently known EGP, one may hope that our predictions and those of others will aid observers in making the much needed detailed observations of EGPs.

We would like to thank Tristan Guillot, Adam Showman and Jean-Pierre Caillault for providing valuable comments and suggestions which greatly improved this paper. Travis Barman would especially like to thank everyone at CRAL, where a large part of this work was carried out. Their hospitality was greatly appreciated. This research was supported by the CNRS and NASA ATP grant NAG 5-3018, NAG 5-8425, LTSA grant NAG 5-3619 to the University of Georgia and LTSA grant NAG5-3435 and NASA EPSCor grant to Wichita State. Some of the calculations presented in this paper were performed on the IBM SP2 at

the UGA UCNS and on the IBM SP2 of the San Diego Supercomputer Center (SDSC), with support from the National Science Foundation, and on the IBM SP2 of the NERSC with support from the DoE. We thank all these institutions for a generous allocation of computer time.

REFERENCES

- Allard, F., Hauschildt, P. H., Alexander, D. R., Tamanai, A., & Schweitzer, A. 2001, *ApJ*, submitted
- Allard, F., Hauschildt, P. H., & Schwenke, D. 2000, *ApJ*, 540, 1005
- Borysow, A. & Frommhold, L. 1986a, *ApJ*, 311, 1043
- . 1986b, *ApJ*, 303, 495
- . 1986c, *ApJ*, 304, 849
- . 1987a, *A&A*, 320, 437
- . 1987b, *ApJ*, 318, 940
- Borysow, A., Jorgensen, U. G., & Cheng. 1997a, *A&A*, 324, 185
- . 1997b, *A&A*, 324, 185
- Borysow, A. & Tang. 1993, *Icarus*, 105, 175
- Brett, J. M. & Smith, R. C. 1993, *MNRAS*, 264, 641+
- Cameron, A., Horne, K., Penny, A., & James, D. 1999, *Nature*, 402, 751
- Chabrier, G., Baraffe, I., Allard, F., & Hauschildt, P. 2000, *ApJ*, 542, 464
- Charbonneau, D., Brown, T. M., Latham, D. W., & Mayor, M. 2000, *ApJ*, 529, L45
- Charbonneau, D., Noyes, R. W., Korzennik, S. G., Nisenson, P., Jha, S., Vogt, S. S., & Kibrick, R. I. 1999, *ApJ*, 522, L145
- Chase, M. W., Davis, C. A., Downey, J. R., Frurip, D. J., McDonald, R. A., & Syverud, A. N. 1985, *J. Phys. Chem. Ref. Data*, 14, Sup.1
- Delfosse, X., Forveille, T., Beuzit, J. ., Udry, S., Mayor, M., & Perrier, C. 1999, *A&A*, 344, 897

- Encrenaz, T. 1999, *A&A Rev.*, 9, 171
- Goukenleuque, C., Bézard, B., Joguet, B., Lellouch, E., & Freedman, R. 2000, *Icarus*, 143, 308
- Grossman, L. 1972, *Geochim. Cosmochim. Acta*, 38, 47
- Gruszka, M. & Borysow, A. 1997, *Icarus*, 129, 172
- Guillot, T. 2000, in *IAU Symposium*, Vol. 202, E19–+
- Guillot, T., Burrows, A., Hubbard, W. B., Lunine, J. I., & Saumon, D. 1996, *ApJ*, 459, L35
- Hauschildt, P. H., Allard, F., & Baron, E. 1999, *ApJ*, 512, 377
- Hauschildt, P. H. & Baron, E. 1999, *Journal of Computational and Applied Mathematics*, 102, 41
- Henry, G. W., Marcy, G. W., Butler, R. P., & Vogt, S. S. 2000, *ApJ*, 529, L41
- Henry, T. J. 1998, in *ASP Conf. Ser. 134: Brown Dwarfs and Extrasolar Planets*, 28+
- Husson, N., Bonnet, B., Scott, N., & A., C. 1992, *JQSRT*, 48, 509
- Leggett, S. K., Allard, F., Dahn, C., Hauschildt, P. H., Kerr, T. H., & Rayner, J. 2000, *ApJ*, 535, 965
- Marcy, G. W., Butler, R. P., Vogt, S. S., Fischer, D., & Lissauer, J. J. 1998, *ApJ*, 505, L147
- Marley, M. S., Gelino, C., Stephens, D., Lunine, J. I., & Freedman, R. 1999, *ApJ*, 513, 879
- Partridge, H. & Schwenke, D. W. 1997, *J. Chem. Phys.*, 106, 4618
- Rothman, L. S., Gamache, R. R., Tipping, R. H., Rinsland, C. P., Smith, M. A. H., Chris Benner, D., Malathy Devi, V., Flaub, J.-M., Camy-Peyret, C., Perrin, A., Goldman, A., Massie, S. T., Brown, L., & Toth, R. A. 1992, *JQSRT*, 48, 469
- Samuelson, R. E., Nath, N., & Borysow, A. 1997, *Planetary & Space Sciences*, 45/8, 959
- Saumon, D., Hubbard, W. B., Burrows, A., Guillot, T., Lunine, J. I., & Chabrier, G. 1996, *ApJ*, 460, 993+
- Seager, S. & Sasselov, D. D. 1998, *ApJ*, 502, L157
- . 2000, *ApJ*, 537, 916

Seager, S., Whitney, B. A., & Sasselov, D. D. 2000, *ApJ*, 540, 504

Sudarsky, D., Burrows, A., & Pinto, P. 2000, *ApJ*, 538, 885

Fig. 1.— Temperature structures for the non-irradiated and irradiated planet ($T_{\text{int}} = 500\text{K}$, $\log(g) = 3.5$) when located 0.1 and 0.05AU from a dM5 ($T_{\text{eff}} = 3000\text{K}$). AMES-Cond is shown on the left and AMES-Dusty on the right. The lowest curve in each panel is the non-irradiated structure. The filled symbols refer to different optical depths (τ) at $\lambda = 1.2\mu\text{m}$

Fig. 2.— Abundances of several important condensates for the irradiated (solid lines) AMES-Dusty ($T_{\text{int}} = 500\text{K}$, $\log(g) = 3.5$) planet when located 0.05AU from a dM5. For comparison, the non-irradiated abundances are also shown (dashed line).

Fig. 3.— Above are the spectra corresponding to the structures shown in Fig. 1. For comparison, the spectrum of the dM5 used as the source of irradiation is also shown. All fluxes have been scaled appropriately for the size of the planet (or primary) and have been scaled to a distance of 5 parsecs. AMES-Dusty is shown on top and AMES-Cond on the bottom panel. Note that all spectra have been heavily smoothed reducing the resolution from $\sim 1\text{\AA}$ to $\sim 50\text{\AA}$.

Fig. 4.— Same as Fig. 1, but now for the younger non-irradiated and irradiated planet ($T_{\text{int}} = 1000\text{K}$, $\log(g) = 3.5$) when located 0.01 and 0.005AU from a dM5. AMES-Cond is shown on the left and AMES-Dusty on the right. As in Fig. 1, the lowest curve in each panel is the non-irradiated structure. The filled symbols refer to different optical depths (τ) at $\lambda = 1.2\mu\text{m}$.

Fig. 5.— Above are the spectra for the structures shown in Fig. 4. For comparison, the spectrum of the dM5 is also shown. All spectra have been scaled as indicated in Fig. 3.

Fig. 6.— Structures for the non-irradiated and irradiated ($T_{\text{int}} = 500\text{K}$, $\log(g) = 3.5$) planet when located 1.0, 0.5 and 0.3AU from a G2 primary. The filled symbols refer to different optical depths (τ) at $\lambda = 1.2\mu\text{m}$.

Fig. 7.— Spectra for the structures shown in Fig. 6. All spectra have been scaled and smoothed as indicated in Fig. 3. In both panels, the lowest spectrum (dotted line) corresponds to the non-irradiated planet.

Fig. 8.— Structures for the non-irradiated and irradiated ($T_{\text{int}} = 1000\text{K}$, $\log(g) = 3.5$) planet when located near a G2 primary. AMES-Cond is shown on the left for 0.25, 0.10 and 0.05AU separations and AMES-Dusty is shown on the right for 0.5, 0.25, and 0.15AU separations. The filled symbols refer to different optical depths (τ) at $\lambda = 1.2\mu\text{m}$.

Fig. 9.— Concentrations of several important condensates for the irradiated AMES-Dusty ($T_{\text{int}} = 1000\text{K}$, $\log(g) = 3.5$) planet when located 0.15AU from a G2 primary.

Fig. 10.— Spectra for the structures shown in Fig. 9. All spectra have been scaled and smoothed as indicated in Fig. 3. In both panels, the lowest spectrum (dotted line) corresponds to the non-irradiated planet.

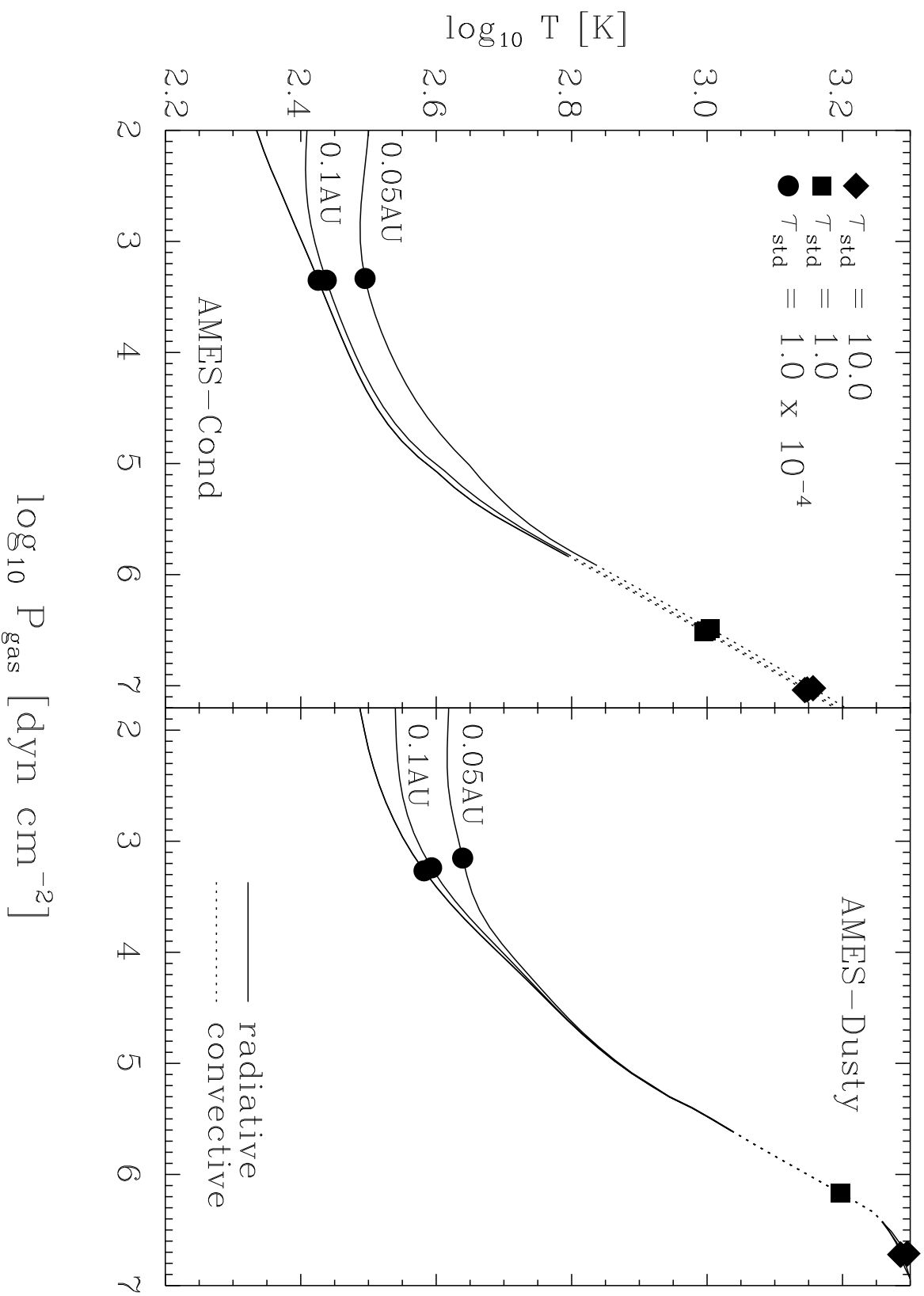
Fig. 11.— Same AMES-Cond spectra as in Figure 10 but focusing on the Na and K doublet features. The spectra have been arbitrarily scaled for comparison.

Fig. 12.— The spectrum for our 1000K AMES-Cond planet located at 0.065AU from a solar type primary is shown above with (solid line) and without (dashed line) the reflected component. Based on the irradiated spectrum without the reflected component, we estimate that $T_{\text{eq}} = 1560\text{K}$. We also show a non-irradiated (AMES-Cond, $T_{\text{eff}} = T_{\text{eq}}$) model with (dotted line) and without (dashed-dotted line) a reflected component. Clearly the hotter non-irradiated model is a poor substitute for the true irradiated case.

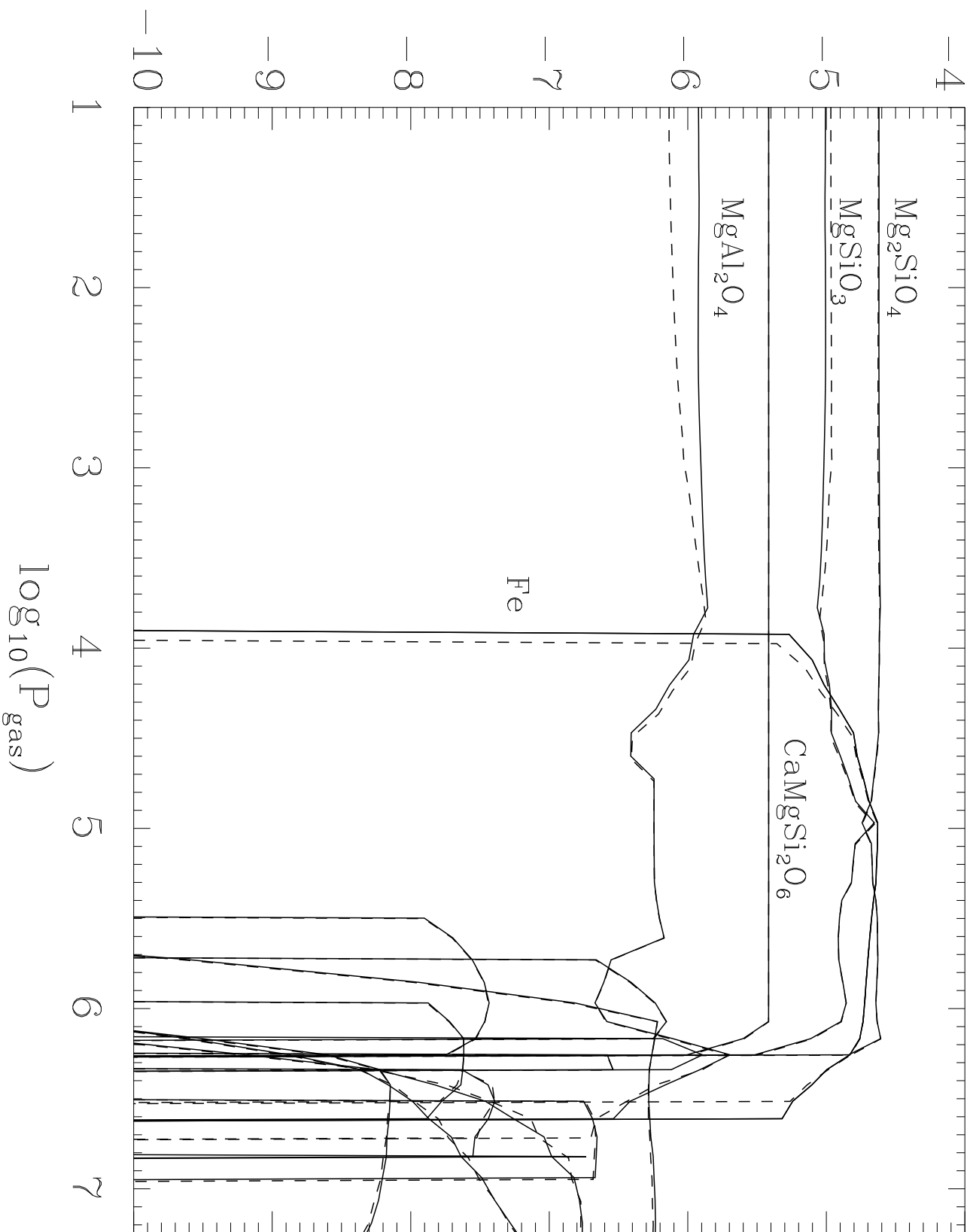
Fig. 13.— The structures for our 1000K AMES-Cond planet located 0.065AU from a solar type primary (top solid line) is compared to a non-irradiated structure of an AMES-Cond planet with $T_{\text{eff}} = T_{\text{eq}} = 1560\text{K}$ (dashed line). The errors which result from assuming a non-irradiated structure are quite apparent at *all* depths. For comparison, the non-irradiated 1000K AMES-Cond planet is also shown (bottom solid line). The filled symbols refer to different optical depths (τ) at $\lambda = 1.2\mu\text{m}$.

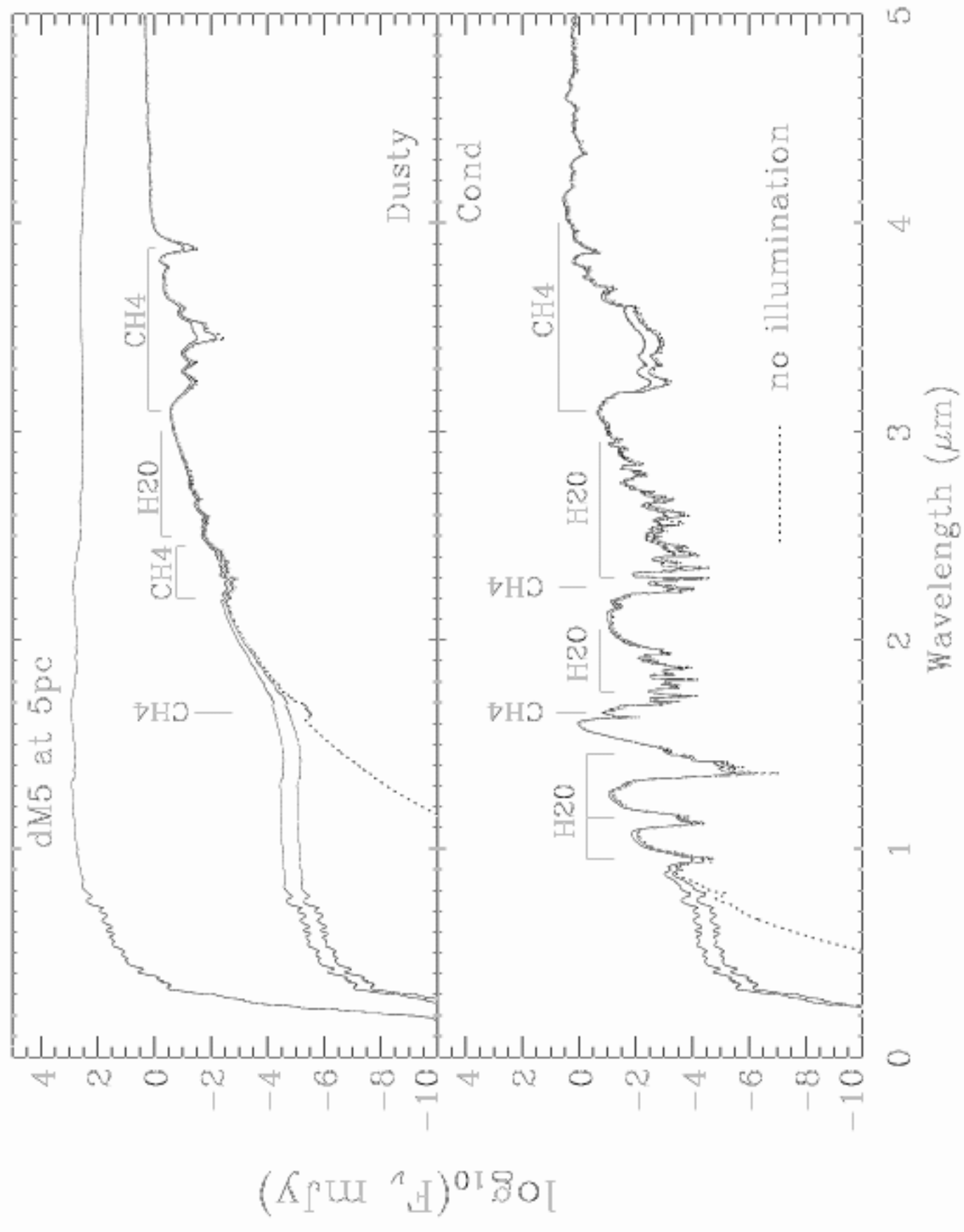
Fig. 14.— The optical spectrum of a $T_{\text{int}} = 1000\text{K}$ planet (dotted line) located at 0.15AU from a G2 primary is compared to the incident stellar spectrum (solid line). The top panel shows the comparison for a Dusty atmosphere and the Cond case is shown in the lower panel. The flux has been arbitrarily scaled to facilitate the comparison.

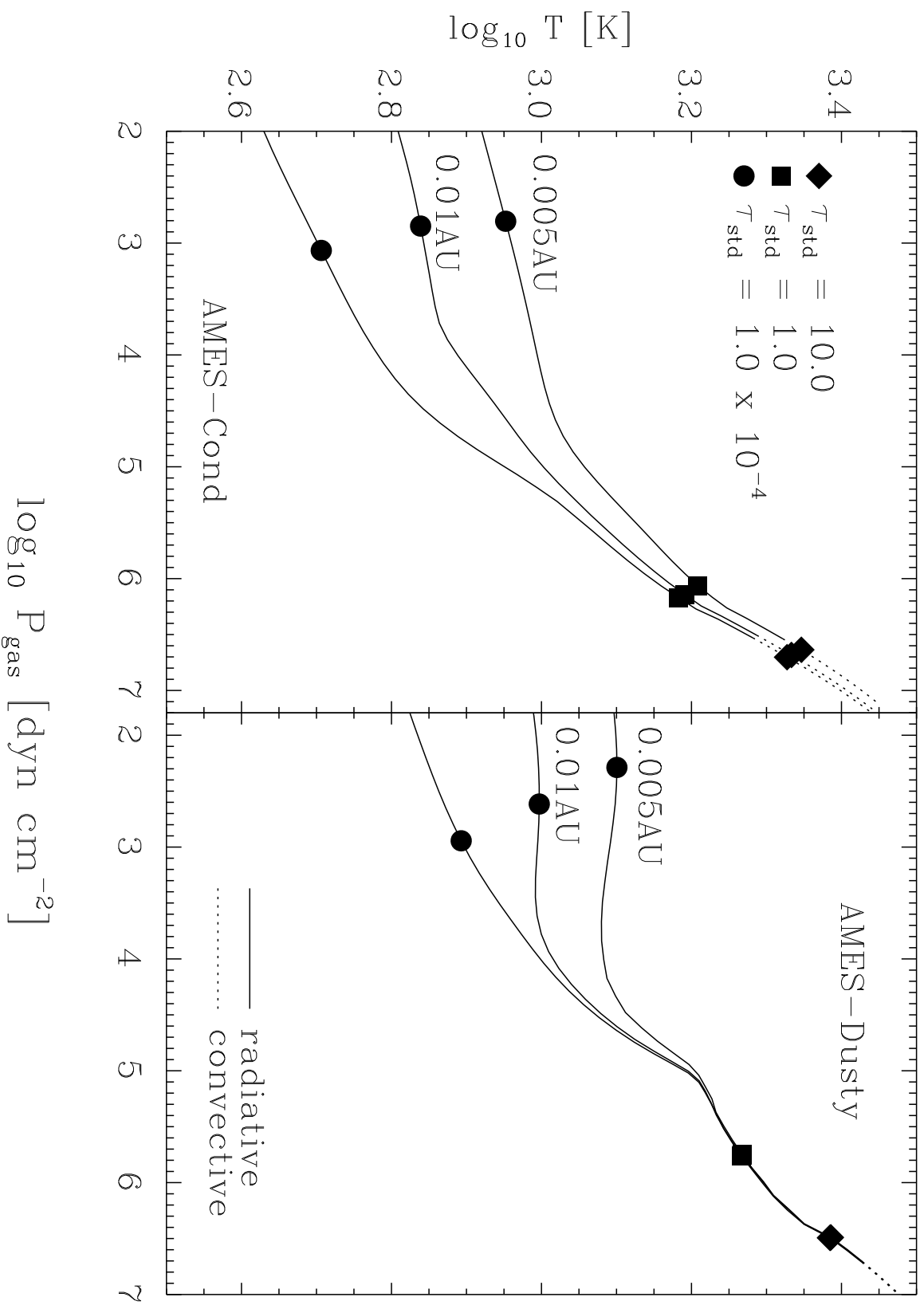
Fig. 15.— The transmitted flux through the limb of a 1000K AMES-Cond planet located 0.05AU from a G2 primary. The second spectrum(full line) is the transmitted flux through our irradiated atmosphere. The bottom spectrum(dotted line) is the transmitted flux through our non-irradiated atmosphere. All spectra have been scaled to 15pc. For comparison, the spectrum of a G2 (top line scaled by an additional 10^{-4}) is also shown. If the deposited energy is not globally redistributed on short time-scales, then the transmitted flux should be closer to the non-irradiated case. Reality is likely to be somewhere in between.

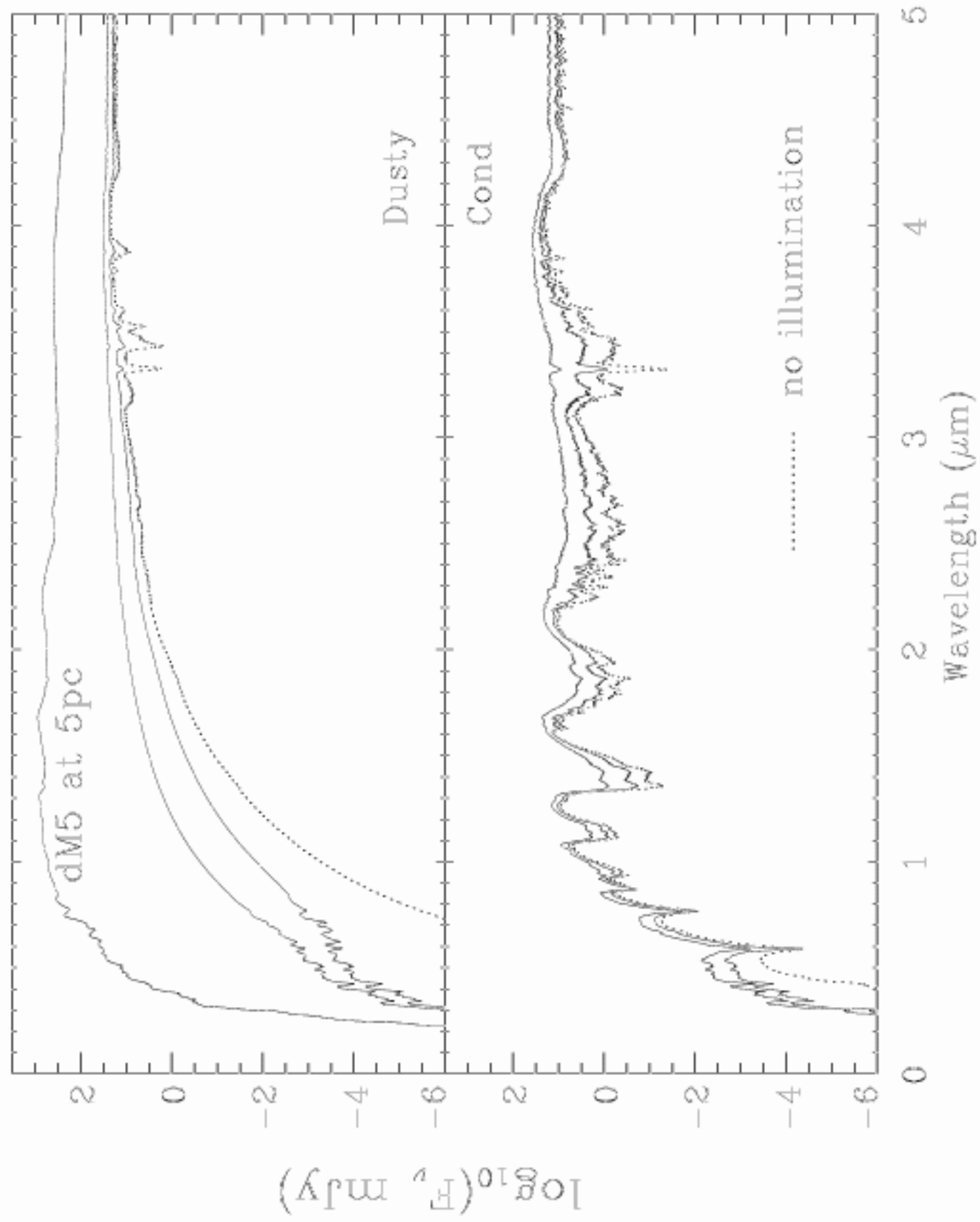


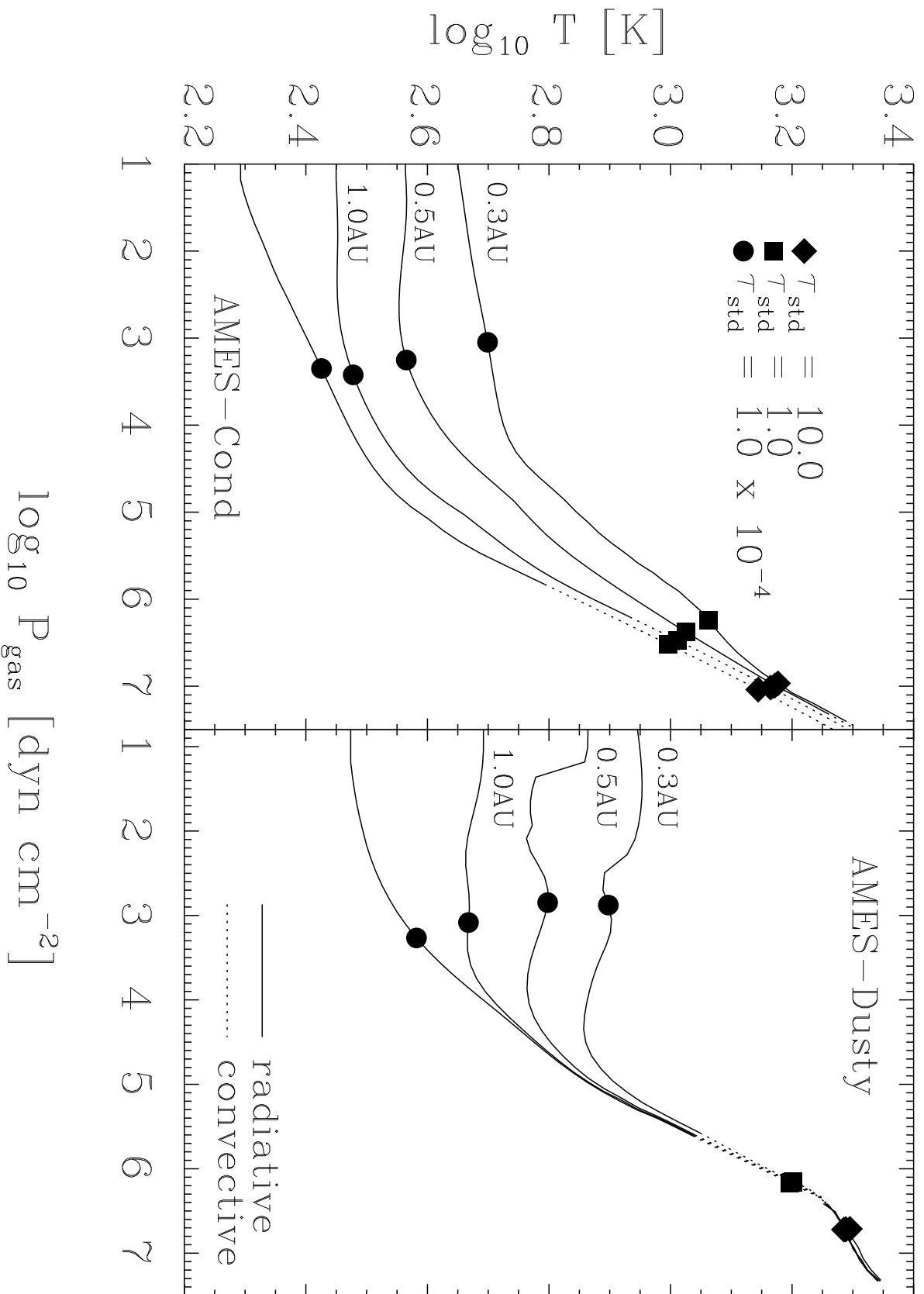
$\log_{10}(P / P_{\text{gas}})$

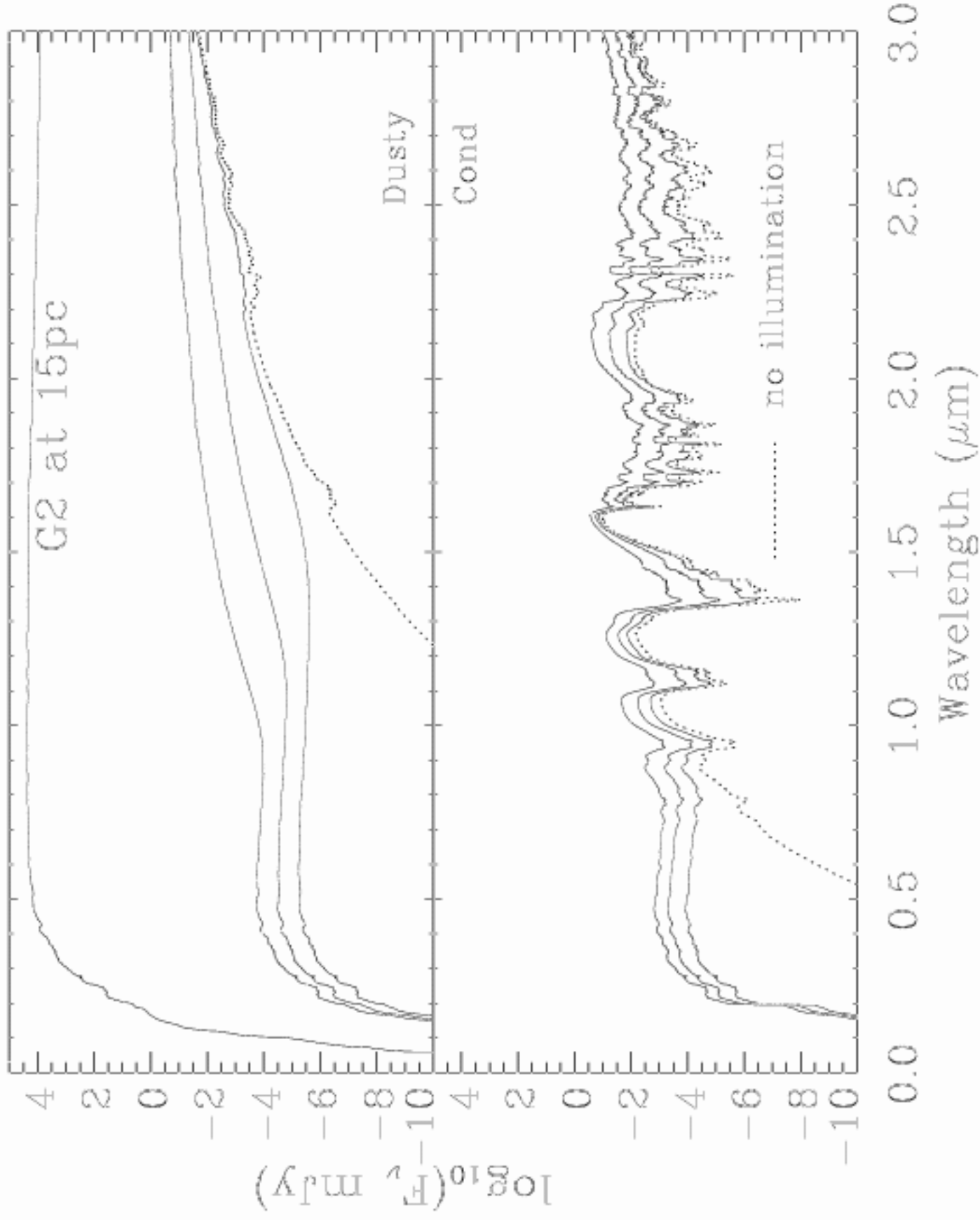


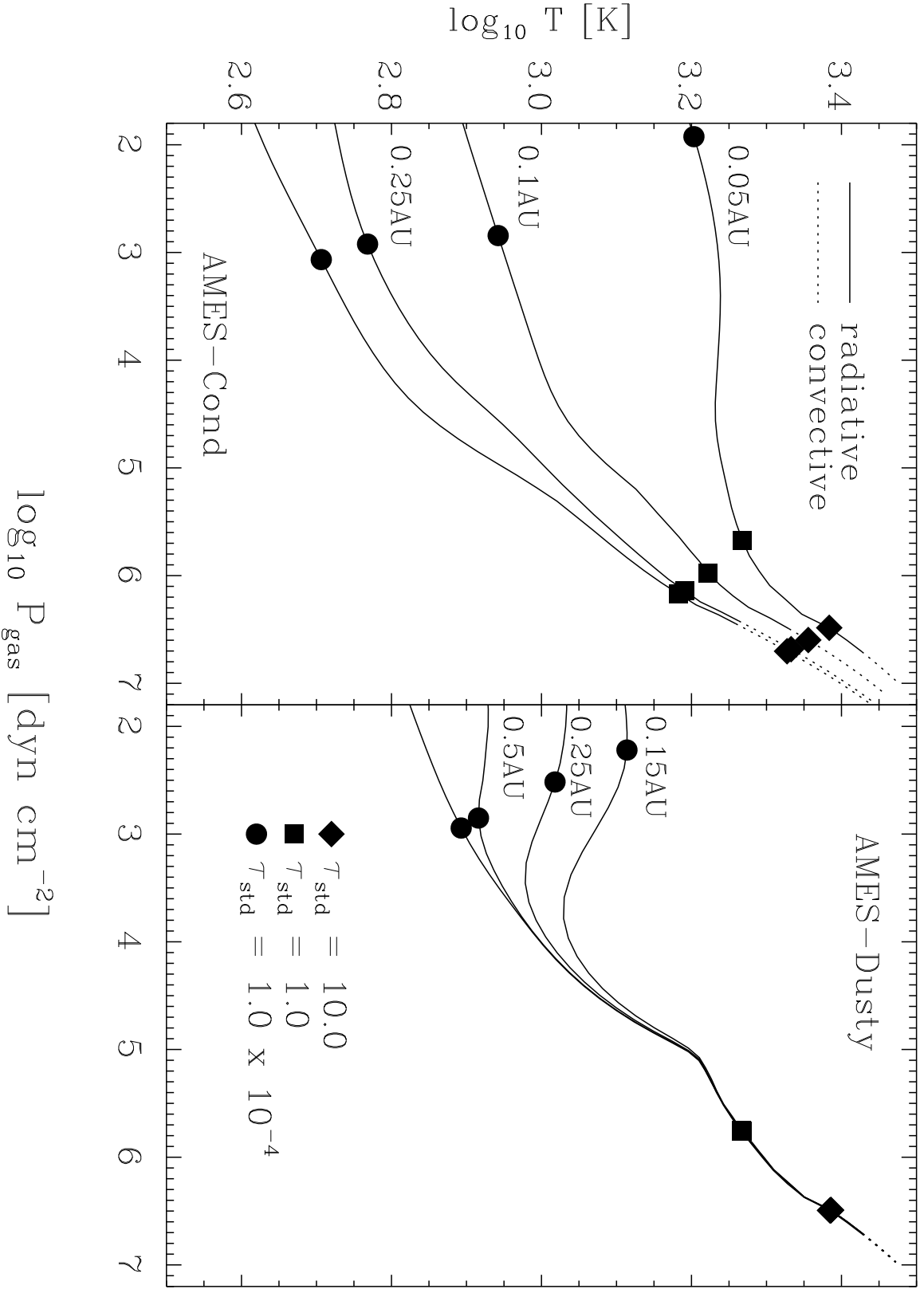


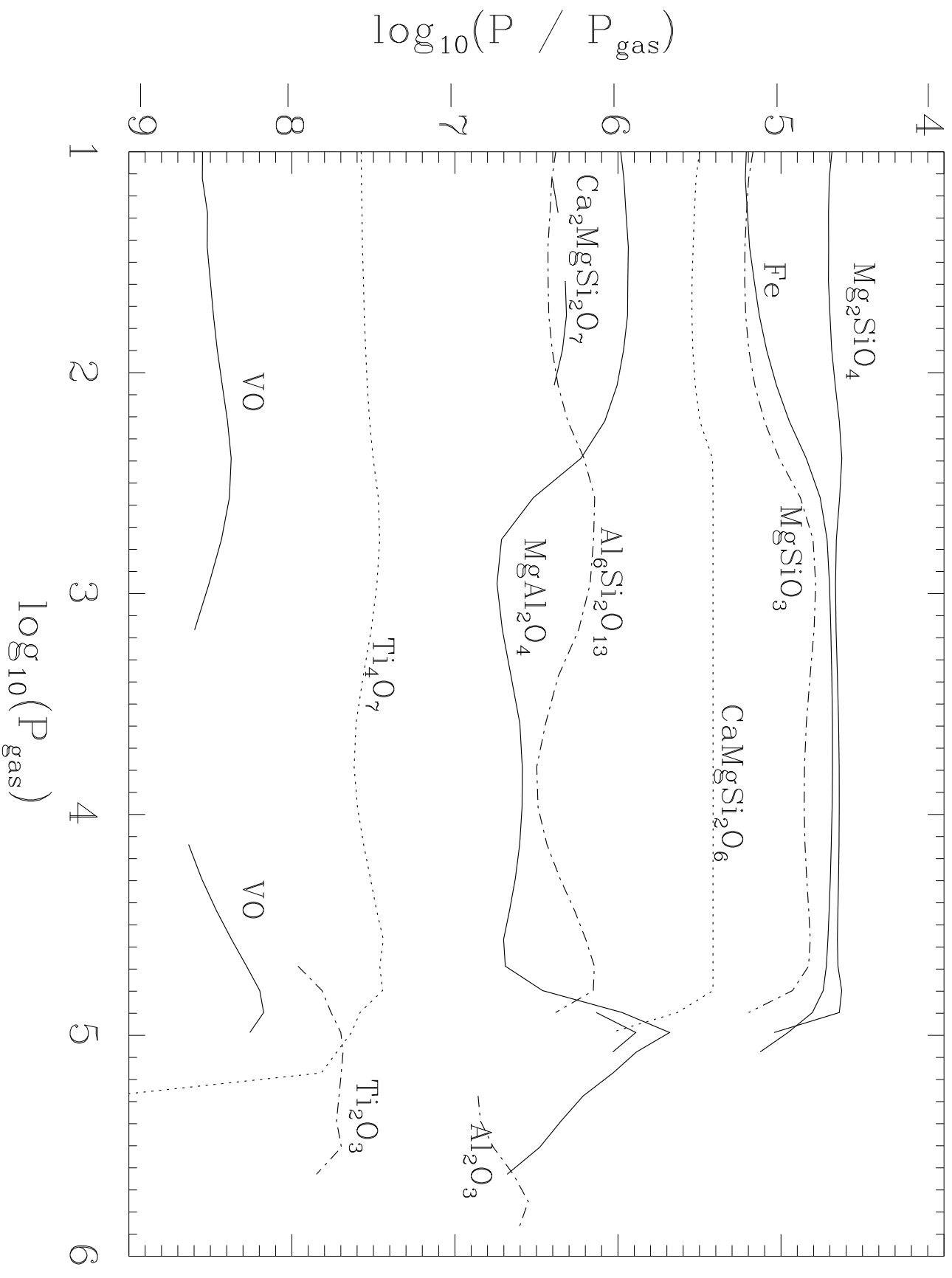


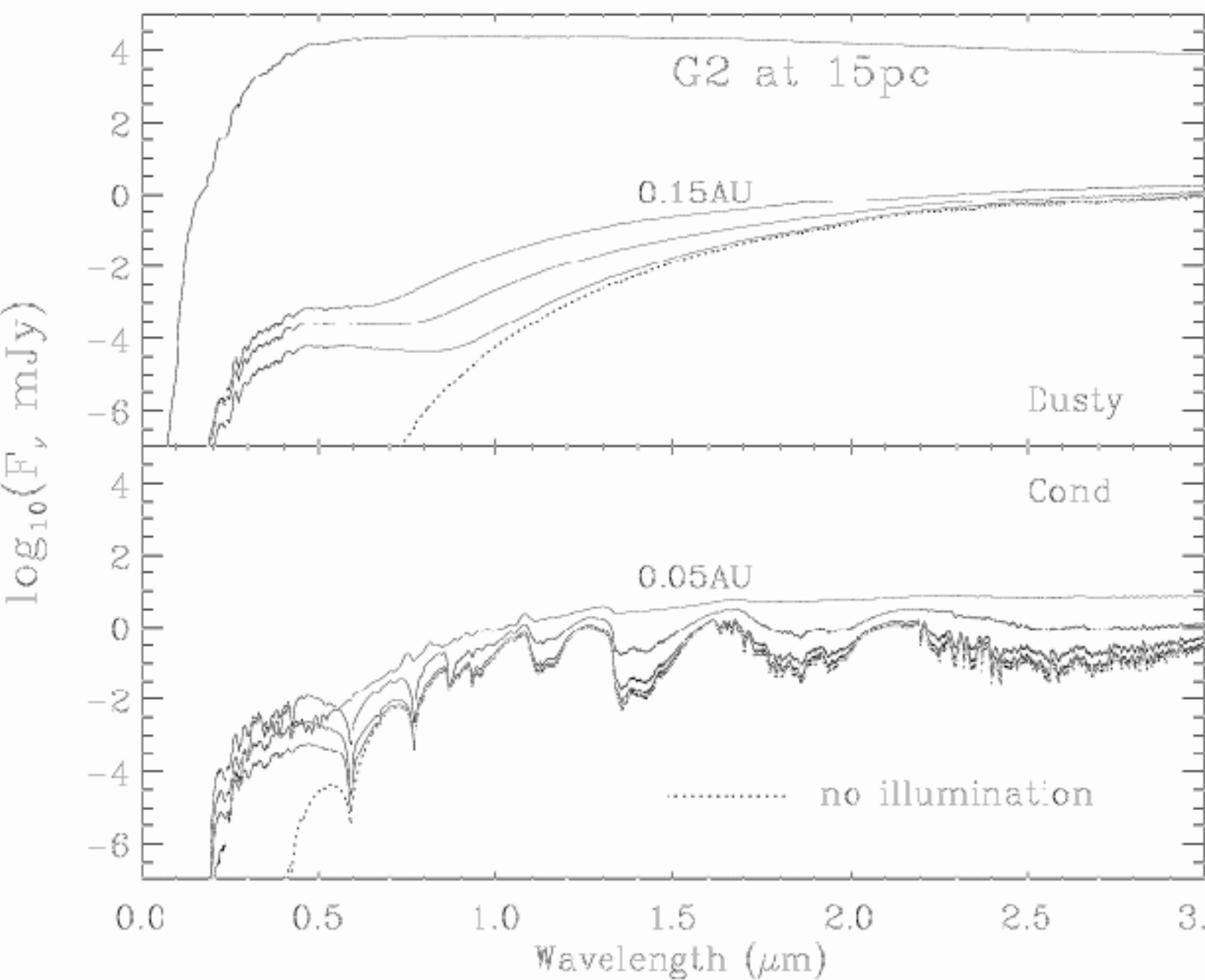


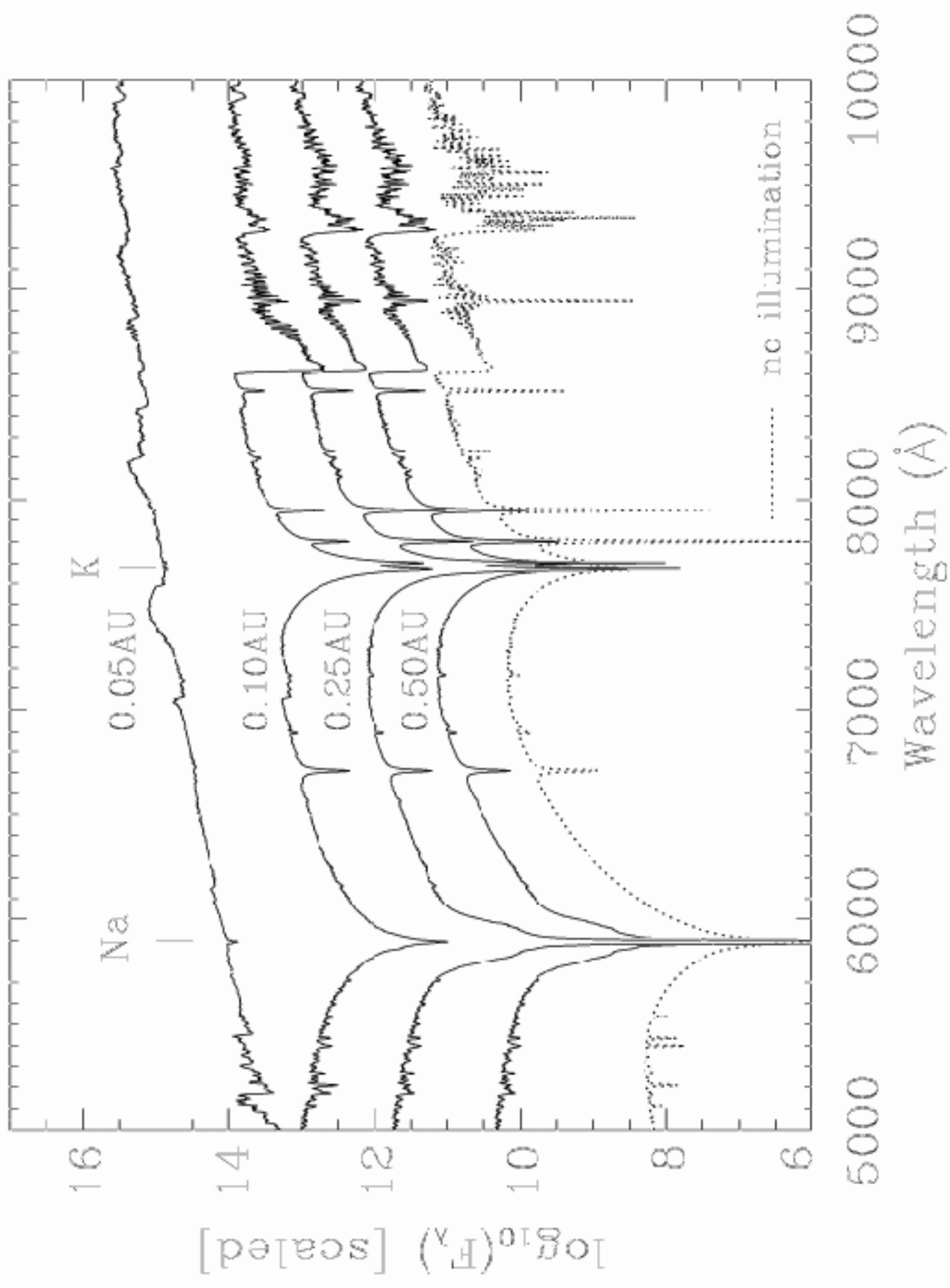


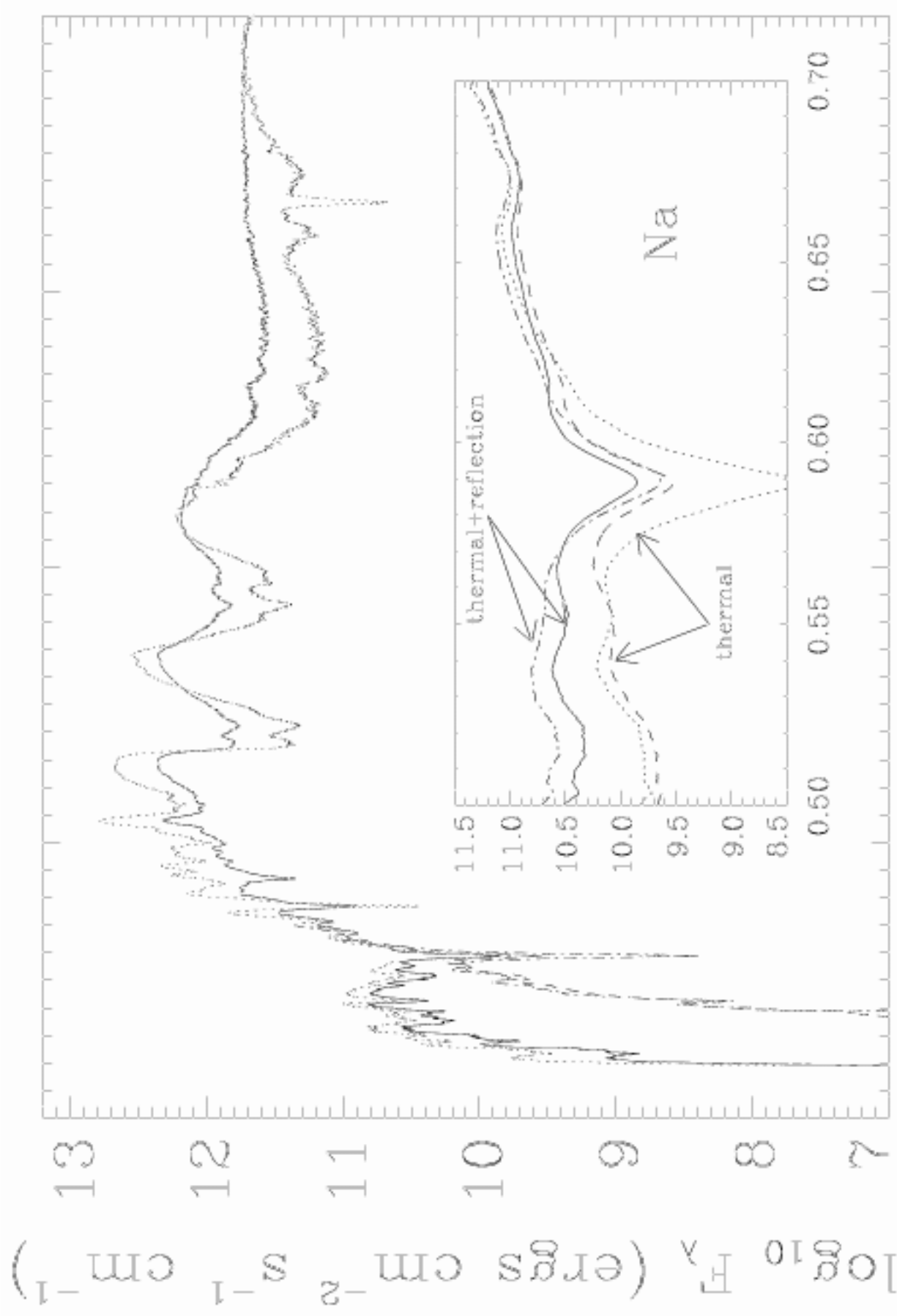












0 1 2 3 4
Wavelength (μm)

